Proceedings of the 2nd World Congress on Recent Advances in Nanotechnology (RAN'17)
Barcelona, Spain – April 4 – 6, 2017
Paper No. NDDTE 125
ISSN: 2371-5308
DOI: 10.11159/nddte17.125

Optimization of Micromagnetic Separation for Bacteremia Treatment

Stephen Petty Valenzuela, Sinead Miller, Charleson Bell, Todd Giorgio
Department of Biomedical Engineering, Vanderbilt University
Nashville, TN, USA
stephen.n.petty.valenzuela@vanderbilt.edu; sinead.e.miller@vanderbilt.edu; c.s.bell@vanderbilt.edu; todd.d.giorgio@vanderbilt.edu

Abstract – Bacteremia and related syndromes such as sepsis and septic shock are becoming an increasing health concern due in large part to the rise of antibiotic resistance and unmet challenges for rapid diagnosis. Extracorporeal bacterial separation methods are currently under development to identify pathogens and reduce the bacterial load. Previous studies have generated models to understand the progression of bacteremia. Here, a physiologically-based pharmacokinetic model was integrated with a physically-based magnetic separation model to inform the design of a micromagnetic separation device. This modeling demonstrates that small-footprint microfluidic devices are not efficient enough for bacteremia treatment in large living systems and further research into high-throughput extracorporeal blood-cleansing devices is required.

***Keywords*:** Bacteremia, magnetic separation, microspheres, optimization

1. Introduction

Bacteremia is defined as the presence of bacteria in the blood, usually from an infection source within a tissue. The immune response to the bacteria and their endotoxins results in life-threatening organ dysfunction, which is known as sepsis[1]. In most developed countries, the incidence of sepsis is estimated to be between 50 and 100 cases per 100,000 people; this incidence is increasing in excess of population growth[2]. Given the complexity of the host-pathogen interactions and the number of infectious pathogens, there is no "gold standard" diagnostic or treatment for sepsis. Initial treatments for the infection are usually broad-spectrum antibiotics and have to be administered soon after diagnosis; with each hour antibiotic therapy is delayed, survival decreases by about 8%[3]. However, more and more pathogenic bacteria have developed resistances to broad-spectrum antibiotics, reducing treatment efficacy. For this model, *Acinetobacter baumannii*, a Gram-negative coccobacillus, was chosen, since it has strong multi-drug resistant phenotypes and is commonly found in clinical settings, causing large nosocomial outbreaks[4].

True treatment of bacteremia involves removing the source of the bacteria. However, infections from blood-borne pathogens are inherently difficult to treat due to their spread from an initial infection site to other locations via the bloodstream; more specifically, the lungs, the liver, and the spleen suffer the greatest burden in bacteremia[5,6]. The removal of bacteria from the various infected organs can be modeled as a clearance mechanism, lending credence to a multi-compartmental physiologically-based pharmacokinetic (PBPK) model. PBPK models of bacterial infection have been in existence since Cheewatrakoolpong et al.'s two-compartmental murine model[7]. Miller et al. were the first to incorporate an extracorporeal pathogen removal device into an infection model[8]. A magnetic separation model was developed by Kang et al. for their device, interrogating the role of the radius of their magnetic beads in separation efficiency from whole blood[9]. Combining these models allows for better understanding of the pharmacokinetics of extracorporeal pathogen removal via magnetic beads and can inform the selection of bead radius, incubation times, and device flow rates.

To calculate the motion, and, thus, the separation, of paramagnetic particles, the magnetic field used must be understood. Specifically, the force on paramagnetic particles is directly proportional to the magnetic flux density gradient. The partial differential equations (PDEs) that describe the magnetic field and magnetic flux density cannot be solved

analytically if complex geometries are involved, such as multiple magnets. The field of the magnets to be used in the separation device were explored in various configurations to optimize the separation of paramagnetic particles.

2. Methods

2.1. Magnetic field modeling

The program FEMM 4.2 was used to calculate the magnetic field, **H**, and flux density, **B**, of the magnets. The general time-invariant magnetostatic problem has the governing equations

$$\nabla \times \mathrm{H} = \mathrm{J} \tag{1}$$

$$\nabla \cdot \mathrm{B} = 0 \tag{2}$$

where **J** is the current density. The constitutive equation relating the field to the flux density by the permeability, μ,

$$\mathrm{B} = \mu \mathrm{H} \tag{3}$$

must be used for each linear material in the domain. FEMM solves these equations using a magnetic vector potential approach, defining the magnetic flux density in terms of a vector potential, **A**,

$$\mathrm{B} = \nabla \times \mathrm{A} \tag{4}$$

This allows the magnetic field governing equation to be rewritten as

$$\nabla \times \left(\frac{1}{\mu} \nabla \times \mathrm{A}\right) = \mathrm{J} \tag{5}$$

and **A** can be solved for using finite element analysis (FEA). **B** and **H** can then be derived from **A**.

Two rectangular neodymium (NdFeB) magnets (K&J Magnetics, BX04X0, Grade N42 NdFeB, 1" x 1/4" x 1" thick, $\mu_r = 1.05,\ H_c = \ 1006582\ \mathrm{A/m}$) were simulated via FEA in an attracting figuration with a separation distance of 25mm, where the microfluidic channels would be. The poles of these magnets are located on the thinner sides rather than on the square faces, making them ideal for a low-profile separator. The flux density field across the gap in the y-direction were obtained and then differentiated in Matlab 2015a to determine the magnetic flux density gradient, represented here as $|\nabla B^2|$.

2.2. Magnetic separation model

The binding efficiency of particles to *A. baumannii* was first estimated. As discussed by Kang et al.[9], the concentration of bound bacteria, c_0, as a function of microsphere radius and incubation time is given by

$$\boldsymbol{c_0(r_b, t_{inc}) = c_0^{in} \exp(-c_e(k_d + k_{shear}) b t_{inc})} \tag{6}$$

where c_0^{in} is the initial concentration of bacteria; c_e is an empirical constant to account for changes in binding efficiency in biologically relevant fluids; k_d and k_{shear} are the collision rate constants of diffusion and shear, given respectively by

$$\mathrm{k_d} = \frac{2\mathrm{r_c k_B T}}{3\eta \mathrm{r_b}} \tag{7}$$

$$\mathrm{k_{shear}} = \pi\dot{\gamma}(\mathrm{r_b} + \mathrm{r_c})^3 \tag{8}$$

with Boltzmann's constant, k_B, the ambient temperature, T, the viscosity of blood, η, the spherical radius of the cell, r_c, and the empirically determined shear rate, $\dot{\gamma}$, held constant; b as the concentration of microspheres calculated relative to a given concentration of r_b = 500 nm microspheres by

$$b = b_{500\ \mathrm{nm}}\left(\frac{500\ \mathrm{nm}}{r_b}\right)^3 \tag{9}$$

and t_{inc} as the incubation time. The overall binding efficiency, x, is therefore calculated as

$$x(r_b, t_{inc}) = 1 - \frac{c_0(r_b, t_{inc})}{c_0^{in}} = 1 - \exp(-c_e(k_d + k_{shear})bt_{inc}) \tag{10}$$

After incubation, the microspheres and microsphere-bacteria complexes are separated out via the magnetophoretic force,

$$F_{mag} = N\frac{4\pi r_b^3}{3}\frac{\chi_v}{2\mu_0}|\nabla B^2| \tag{11}$$

with the constants μ_0, the vacuum magnetic permeability; χ_v, the volumetric susceptibility of the microspheres; and $|\nabla B^2|$, the magnetic flux density gradient. N is the number of microspheres bound to a bacterium and is estimated by

$$N(r_b) = 4\rho\left(\frac{r_c}{r_b}\right)^2 \tag{12}$$

Here, ρ refers to the proportion of the cell surface covered by microspheres.

Opposing the magnetophoretic force is the drag force in terms of the magnetophoretic velocity, v_{mag}, given by Stokes flow

$$F_{drag} = 6\pi r_n \eta v_{mag} \tag{13}$$

where r_n is the effective hydraulic radius of a microsphere-bacterium complex given by

$$r_n = \sqrt[3]{r_c^3 + Nr_b^3} \tag{14}$$

Solving $F_{mag} = F_{drag}$ for v_{mag} under the assumption of force equilibrium, the magnetophoretic velocity of the complexes is equal to

$$v_{mag} = \frac{Nr_b^3\chi_v|\nabla B^2|}{9\eta\mu_0 r_n} \tag{15}$$

Therefore, the magnetic separation time across the width of the channel, w, can be calculated as

$$t_{mag} = w/v_{mag} \tag{16}$$

Assuming steady flow in the separation channels, the average velocity of a complex is given by

$$\overline{v_f} = \frac{Q_E}{nA} \tag{17}$$

Q_E being the volumetric flow rate through the entire device, n being the number of channels, and $A = hw$ being the rectangular cross-sectional area of a channel with height h and width w. The residence time in the channel with length l can be calculated as

$$t_{res} = l/\overline{v_f} \tag{18}$$

The magnetic separation efficiency m is then estimated by

$$m(r_b, Q_E) = \begin{cases} \frac{t_{res}}{t_{mag}} & , t_{res} < t_{mag} \\ 1 & , t_{res} \geq t_{mag} \end{cases} \tag{19a}$$

$$= \begin{cases} \frac{4nhl\rho r_b r_c^2 \chi_v |\nabla B^2|}{9Q_E \eta \mu_0 (r_c^3 + 4\rho r_b r_c^2)^{1/3}} & , t_{res} < t_{mag} \\ 1 & , t_{res} \geq t_{mag} \end{cases} \tag{19b}$$

After the incubation and separation stages, the overall fraction of bacteria removed can be expressed as

$$f(r_b, Q_E, t_{inc}) = x(r_b, t_{inc}) * m(r_b, Q_E) \tag{20}$$

Table 1 lists the physical constants and parameters used for all of the simulations. The device-specific parameters (width, height, length, and number of channels) are based on a microfluidic design currently in use.

Table 1: Constants for magnetic separation efficiency calculations.

Parameter	Value and units	Parameter	Value and units
$\boldsymbol{c_0^{in}}$	10^7 CFU/mL	$\boldsymbol{\chi_v}$	3.5
$\boldsymbol{c_e}$	3.7 x 10^{-4}	$\boldsymbol{\rho}$	0.5
$\boldsymbol{T}$	300 K	$\boldsymbol{w}$	1 x 10^{-4} m
$\boldsymbol{\eta}$	4.0 x 10^{-3} kg m^{-1} s^{-1}	$\boldsymbol{n}$	2
$\boldsymbol{r_c}$	0.5 x 10^{-6} m	$\boldsymbol{h}$	5 x 10^{-5} m
$\boldsymbol{\dot{\gamma}}$	1.0186 s^{-1}	$\boldsymbol{l}$	2.5 x 10^{-2} m
$\boldsymbol{b_{500\ nm}}$	0.0025 kg m^{-3}		

2.2. Physiologically-based pharmacokinetic model

The fractional magnetic separation from Equation 20 factors into the five-compartment PBPK model of infection diagrammed in Fig. 1 and detailed in Equations 21-25. Each physiologic compartment has its own associated growth rate, G_i, a blood volume, V_i, blood flow rate, Q_i, and a partition coefficient to bacteria, p_i (Table 2). The transport of bacteria between compartments is represented by the arrows in Figure 2. The most significant modification from the model

published by Miller et al.[8] is the removal of the return pathway from the device to the blood; here, the assumption is that any bacteria removed by the device has no path of reentry into the circulatory system.

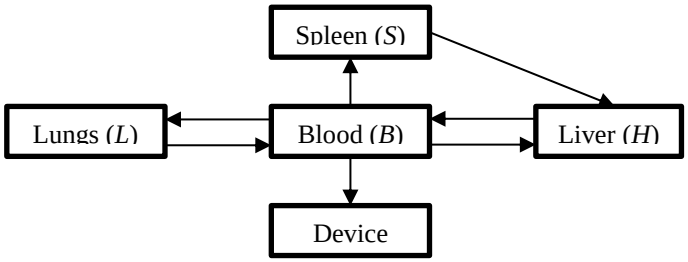

Fig. 1: Diagram of infection compartmental model. Arrows indicate blood flow between the compartments. Letters in parentheses indicate symbols used for the compartmental concentrations in the equations.

$$\frac{dL}{dt} = G_L L + \frac{Q_L}{V_L} B - \frac{Q_L}{\mathrm{p}_L V_L} L \tag{21}$$

$$\frac{dS}{dt} = G_S S + \frac{Q_S}{V_S} B - \frac{Q_S}{\mathrm{p}_S V_S} S \tag{22}$$

$$\frac{dH}{dt} = G_H H + \frac{Q_H}{V_H} B + \frac{Q_S}{\mathrm{p}_S V_S} S - \frac{Q_H + Q_S}{\mathrm{p}_H V_H} H \tag{23}$$

$$\frac{dB}{dt} = G_B B + \frac{Q_H + Q_S}{\mathrm{p}_H V_H} H + \frac{Q_L}{\mathrm{p}_L V_L} L - \left(\frac{Q_L}{V_L} + \frac{Q_S}{V_S} + \frac{Q_H}{V_H} + f(r_b, Q_E, t_{inc}) \frac{Q_E}{V_E}\right) B \tag{24}$$

$$\frac{dE}{dt} = f(r_b, Q_E, t_{inc}) \frac{Q_E}{V_E} B \tag{25}$$

Six different infection and treatment scenarios were then simulated using the coupled models: a non-immunocompromised human, an immunocompromised human, an immunocompromised human with antibiotic administration, and using the extracorporeal device with the three previous scenarios. A simulated bolus of 10^7 CFU/mL of *A. baumannii* was injected into the lung compartment and allowed to proliferate in the system for ten hours. After incubating the blood with the colistinated magnetic microspheres for $t_{inc} = 5$ min, the extracorporeal device was linked into the system and ran for 96 hours. To determine the efficacy of treatment, the area under the curve (AUC) via trapezoidal integration in each of the compartments was compared across flow rates and microsphere radii. As a quantifiable criterion, the time to go below a threshold of 1 CFU/mL in the bloodstream was also examined[8].

Matlab 2015a's 4th-order Runge-Kutta solver was used to calculate an approximate solution to the system of differential equations.

Table 2: Parameters for PBPK model of *A. baumannii* infection.

IC = immunocompromised AB = antibiotic + immunocompromised			p_i		G_i (h^{-1})		
Compartment	Q_i ($m^3\ h^{-1}$)	V_i ($m^3\ h^{-1}$)	Normal	IC	Normal	IC	AB
Lungs	0.08995	4.50×10^{-4}	93	3	-1.74	0.21	-0.24
Spleen	0.01501	2.09×10^{-4}	59	28	-0.14	0.14	-0.07
Liver	0.0483	1.56×10^{-3}	749	79	-0.10	0.10	-0.18
Blood	N/A	N/A	N/A	N/A	-0.17	0.08	-0.05
Device	variable	2.5×10^{-10}	1	1	N/A	N/A	N/A

3. Results and discussion

3.1. Magnetic field modeling

The domain around two rectangular NdFeB magnets was simulated with 4574 nodes and 8721 elements via FEA. The calculated two-dimensional magnetic flux density agrees with the manufacturer's documentation (Fig. 2a). A parabolic profile with a maximum flux density of 0.521T and a minimum field strength of 0.360T was achieved across the channel (Fig. 2b). The magnetic flux density gradient ranges from approximately -20 T^2/m to 20 T^2/m; discretization error from differentiation resulted in a non-smooth curve (Fig. 2c). At the location of the microfluidic channels, 2.1mm from the center of the space between the magnets, the magnetic flux density gradient was estimated to be 4.7 T^2/m. With this magnetic flux field, a linear magnetic flux density gradient can be established to ensure consistent separation of magnetic complexes.

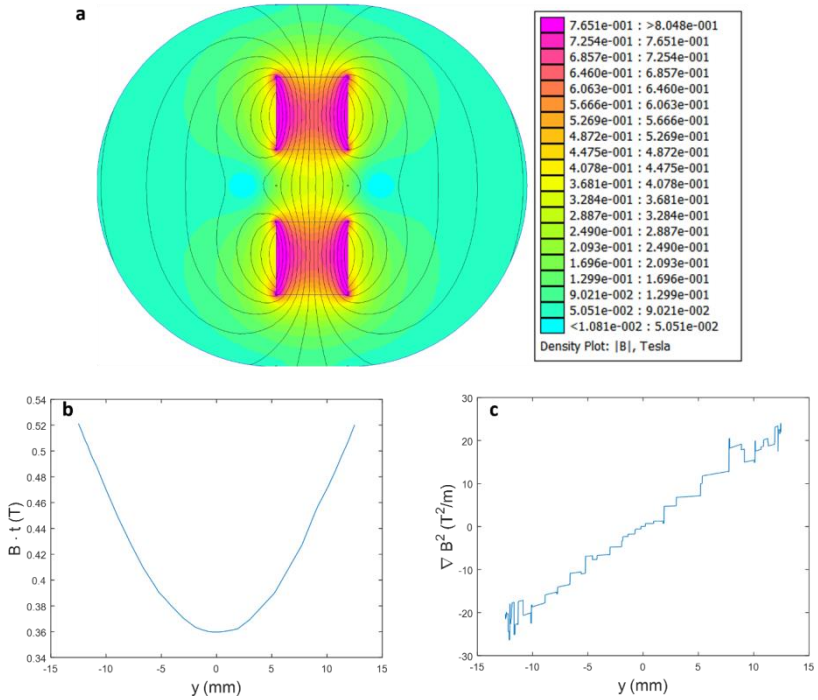

Fig. 2: Finite element analysis results of the magnetic field between two NdFeB magnets. The magnetic field strength (a) is consistent with the manufacturer's results. The magnetic field strength between the two magnets has a parabolic profile (b). Therefore, a linear magnetic flux density gradient was to be expected (c).

3.2. Physiologically-based pharmacokinetic model with magnetic separation

Using the magnetic flux density gradient from the previous magnetostatic simulation, the magnetic separation of microsphere-bacteria complexes was modeled for microspheres with radii from 25nm to 500nm, which correspond to common paramagnetic microspheres. The device flow rate was varied over the typical range of microfluidic flow rates, 0.01mL/min to 1.5mL/min. No significant change was seen with the infection metrics in any immune situation (Table 3), despite consistent capture of bacteria (Fig. 3).

Table 3: Infection metrics, including maximum bacterial load, time to threshold, and area under the curve, did not change significantly with varied microsphere radius or flow rate (mean ± standard deviation). The standard deviation of any metric is at least two orders of magnitude smaller than the mean. N/A here indicates that the compartment's bacterial load never went below 1 CFU/mL.

	Compartment	Max. load (CFU/mL)	Time to threshold (h)	AUC (CFU/mL * h)
Non-immunocompromised	Lungs	$1.32 \times 10^{4} \pm 6.82 \times 10^{-10}$	75.97 ± 0.001	$1.06 \times 10^{5} \pm 8.09 \times 10^{0}$
	Spleen	$1.45 \times 10^{4} \pm 4.02 \times 10^{-10}$	76.72 ± 0.002	$1.16 \times 10^{5} \pm 8.33 \times 10^{0}$
	Liver	$8.66 \times 10^{5} \pm 5.47 \times 10^{-9}$	N/A	$6.93 \times 10^{6} \pm 9.73 \times 10^{1}$
	Blood	$2.49 \times 10^{2} \pm 2.63 \times 10^{-2}$	44.17 ± 0.004	$1.99 \times 10^{3} \pm 1.57 \times 10^{-1}$
Immunocompromised	Lungs	$1.02 \times 10^{10} \pm 5.36 \times 10^{7}$	N/A	$9.58 \times 10^{10} \pm 4.57 \times 10^{8}$
	Spleen	$9.61 \times 10^{10} \pm 5.04 \times 10^{7}$	N/A	$9.04 \times 10^{11} \pm 4.29 \times 10^{9}$
	Liver	$6.76 \times 10^{11} \pm 3.48 \times 10^{9}$	N/A	$6.36 \times 10^{12} \pm 2.96 \times 10^{10}$
	Blood	$3.39 \times 10^{9} \pm 1.78 \times 10^{7}$	N/A	$3.19 \times 10^{10} \pm 1.52 \times 10^{8}$
+ Antibiotic immunocompromised	Lungs	$2.48 \times 10^{4} \pm 5.71 \times 10^{-10}$	60.76 ± 0.02	$1.49 \times 10^{5} \pm 6.44 \times 10^{1}$
	Spleen	$2.41 \times 10^{5} \pm 4.83 \times 10^{-9}$	74.41 ± 0.03	$1.44 \times 10^{6} \pm 5.87 \times 10^{2}$
	Liver	$1.66 \times 10^{4} \pm 5.26 \times 10^{-10}$	86.00 ± 0.03	$9.94 \times 10^{6} \pm 3.13 \times 10^{3}$
	Blood	$8.27 \times 10^{3} \pm 1.55 \times 10^{-10}$	54.17 ± 0.02	$4.96 \times 10^{4} \pm 2.15 \times 10^{1}$

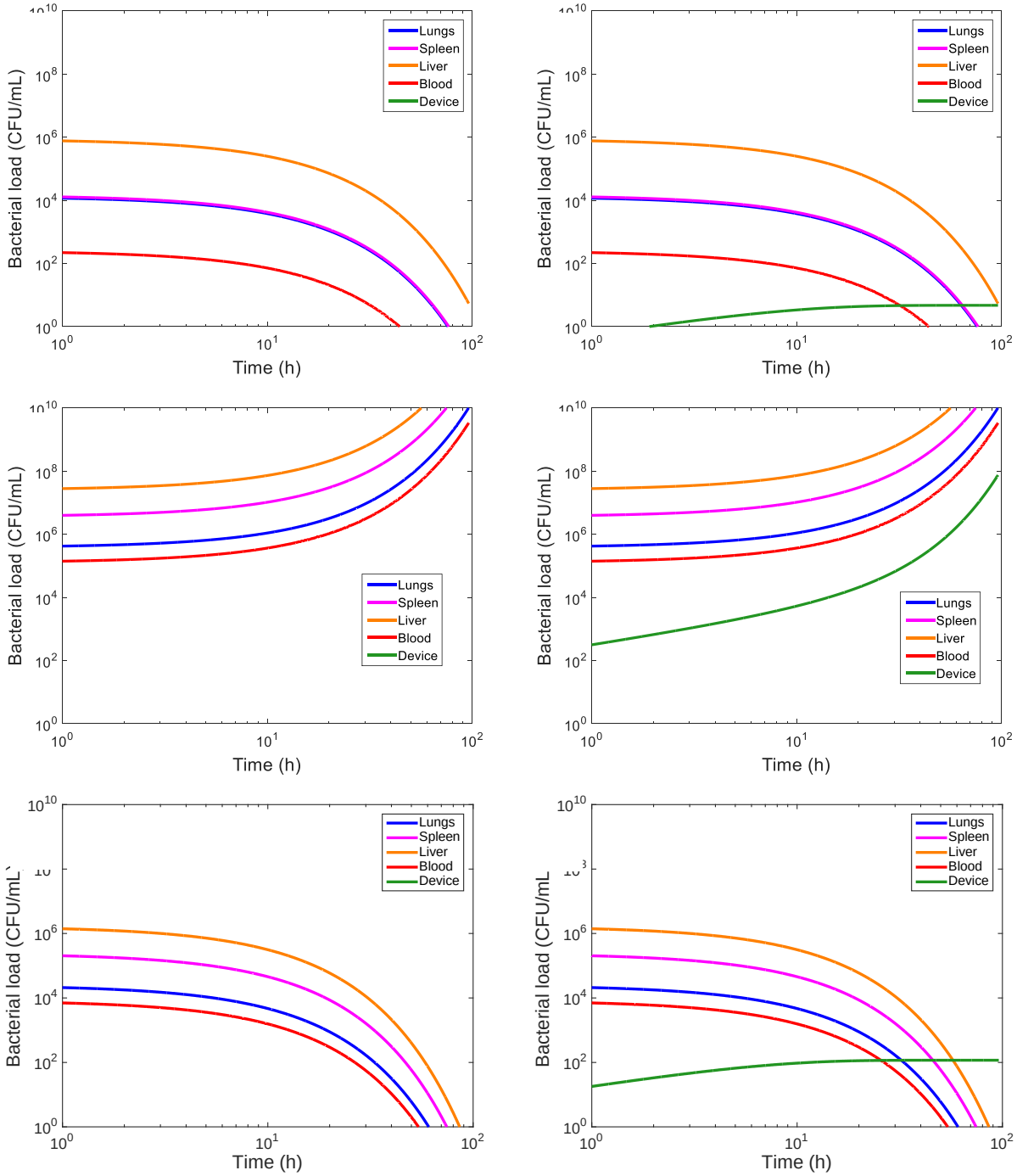

Fig. 3: Log-log plots of bacterial load over time for all compartments with r_b = 75 nm and Q_E = 0.1 mL/min. From top to bottom: non-immunocompromised (a, b), immunocompromised (c, d), and immunocompromised with antibiotic (e, f). Bacterial loads do not change significantly with the incorporation of the extracorporeal device, despite quantifiable bacterial capture (b, d, f), in comparison with the absence of extracorporeal bacterial separation (a, c, e).

4. Conclusion

Incorporating a physically-based magnetic separation efficiency model into a physiologically-based pharmacokinetic model allows for a better understanding of the efficacy of a magnetics-based extracorporeal separation device. Here, it is demonstrated that with conventional magnets and microfluidics, clinical outcomes would most likely not improve, since bacterial load metrics were not significantly changed by any change to the microsphere radius or device flow rate. High-throughput, high-capture devices will be essential for there to be any improvement of patient outcomes.

Acknowledgements

This work was supported by the U.S. Department of Defense under contract W81XWH-13-1-0397, Vanderbilt University School of Engineering, and the Vanderbilt University Undergraduate Summer Research Program (VUSRP).

References

[1] C. W. Seymour, V. X. Liu, T. J. Iwashyna, F. M. Brunkhorst, T. D. Rea, A. Scherag, G. Rubenfeld, J. M. Kahn, M. Shankar-Hari, M. Singer, C. S. Deutschman, G. J. Escobar, and D. C. Angus, "Assessment of Clinical Criteria for Sepsis: For the Third International Consensus Definitions for Sepsis and Septic Shock (Sepsis-3)," *Jama*, vol. 315, no. 8, pp. 762–74, 2016.

[2] D. C. (Pitt) Angus, T. van der Poll, D. A. Wacker, M. E. Winters, S. R. Finfer, J.-L. Vincent, D. De Backer, G. S. Martin, M. Mutschler, T. Paffrath, C. Wölfl, C. Probst, U. Nienaber, I. B. Schipper, B. Bouillon, and M. Maegele, "Severe sepsis and septic shock," *Emerg. Med. Clin. North Am.*, vol. 45, Suppl 3, no. 4, pp. 747–758, 2013.

[3] A. Kumar, D. Roberts, K. E. Wood, B. Light, J. E. Parrillo, S. Sharma, R. Suppes, D. Feinstein, S. Zanotti, L. Taiberg, D. Gurka, A. Kumar, and M. Cheang, "Duration of hypotension before initiation of effective antimicrobial therapy is the critical determinant of survival in human septic shock," *Crit Care Med.*, vol. 34, no. 0090–3493, pp. 1589–1596, 2006.

[4] P. E. Fournier, "The Epidemiology and Control of Acinetobacter baumannii in Health Care Facilities HABITAT," vol. 42, 2006.

[5] F. W. Guirgis, S. Brakenridge, S. Sutchu, J. D. Khadpe, T. Robinson, R. Westenbarger, S. T. Topp, C. J. Kalynych, J. Reynolds, S. Dodani, F. A. Moore, and A. E. Jones, "The long-term burden of severe sepsis and septic shock," *J. Trauma Acute Care Surg.*, vol. 81, no. 3, p. 1, 2016.

[6] M. Altamura, L. Caradonna, L. Amati, N. M. Pellegrino, G. Urgesi, and S. Miniello, "Splenectomy and Sepsis: the Role of the Spleen in the Immune-Mediated Bacterial Clearance," *Immunopharmacol. Immunotoxicol.*, vol. 23, no. 2, pp. 153–161, 2001.

[7] B. Cheewatrakoolpong, E. K. Steffen, R. Don Brown, and R. D. Berg, "Kinetic analysis of bacterial clearance in mice using the ESTRIPc and KINET microcomputer programs," *J. Immunol. Methods*, vol. 58, no. 3, pp. 375–381, 1983.

[8] S. E. Miller, C. S. Bell, M. S. Mcclain, T. L. Cover, and T. D. Giorgio, "Dynamic Computational Model of Symptomatic Bacteremia to Inform Bacterial Separation Treatment Requirements," *PLoS One*, vol. 11, no. 9, pp. 1–22, 2016.

[9] J. H. Kang, E. Um, A. Diaz, H. Driscoll, M. J. Rodas, K. Domansky, A. L. Watters, M. Super, H. A. Stone, and D. E. Ingber, "Optimization of Pathogen Capture in Flowing Fluids with Magnetic Nanoparticles," *Small*, vol. 11, no. 42, pp. 5657–5666, 2015.